

# Seismic signatures of two orthogonal sets of vertical microcorrugated fractures

Rodrigo Felício Fuck\* and Ilya Tsvankin, Center for Wave Phenomena, Colorado School of Mines

## Summary

Conventional fracture-characterization techniques operate with the idealized model of penny-shaped (rotationally invariant) cracks and ignore the roughness (microcorrugation) of fracture surfaces. Here, we develop analytic solutions based on the linear-slip theory to examine wave propagation through an effective triclinic medium that contains two microcorrugated, vertical, orthogonal fracture sets in isotropic background rock.

The corrugation of fracture surfaces makes the shear-wave splitting coefficient at vertical incidence sensitive to fluid saturation, especially for tight, low-porosity formations. Also, in contrast to the model with two orthogonal sets of penny-shaped cracks, the NMO (normal-moveout) ellipses of all three reflection modes (P,  $S_1$ ,  $S_2$ ) are rotated with respect to the fracture strike directions. Another unusual property of the fast shear wave  $S_1$  is the misalignment of the semi-major axis of its NMO ellipse and the polarization vector at vertical incidence.

Our model may adequately describe the orthogonal fracture sets at Weyburn Field in Canada, where the axes of the P-wave NMO ellipse deviate from the  $S_1$ -wave polarization direction. The results of this work can be used to identify the underlying physical model and, potentially, estimate the combinations of fracture parameters constrained by multiazimuth, multicomponent seismic data.

## Introduction

Since fluid pathways are often formed by fracture networks and joints, seismic fracture characterization is an important area of reservoir geophysics. Bakulin et al. (2000) outlined several practical approaches to estimating fracture parameters from surface seismic and VSP (vertical seismic profiling) data. These papers, however, are largely focused on the model of rotationally invariant fractures (i.e., oblate spheroids), which have perfectly smooth surfaces and are often called “penny-shaped cracks.” Grechka et al. (2003) considered a single set of the most general fractures allowed by the linear-slip formalism of Schoenberg (1980). Such “general” fractures have rough (microcorrugated) surfaces and are described by a compliance matrix that has nonzero off-diagonal elements. The results of Grechka et al. (2003) show that fracture rheology has a strong impact on the velocities and reflection moveout of both P- and S-waves.

Many naturally fractured reservoirs, however, contain two (or even more) systems of fractures. That is the case, for example, at Weyburn field in Canada, where borehole imaging reveals two dominant fracture sets, which are approximately orthogonal to each other (Cardona,

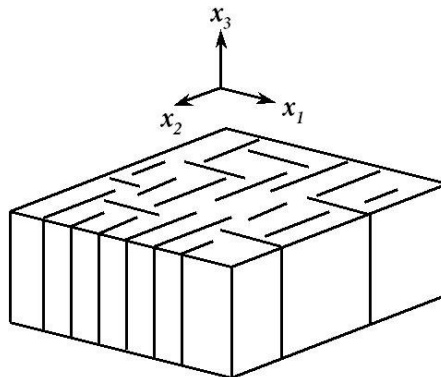


Fig. 1: Model of two sets of orthogonal vertical fractures. The fracture strikes are parallel to the axes  $x_1$  and  $x_2$  of the Cartesian coordinate frame. Note that the linear-slip theory does not account for the interaction of fracture sets.

2002). The assumption that both fracture sets are rotationally invariant cannot explain the misalignment of P-wave NMO ellipses and the fast S-wave polarization direction observed in some parts of the reservoir. Making the fractures microcorrugated can help to develop an effective model that accounts for this anomaly without introducing a third fracture system.

Here, we discuss seismic signatures of two vertical, orthogonal, microcorrugated fracture sets embedded in isotropic background rock (Figure 1). To gain insight into the influence of fracture rheology on seismic wavefields, we apply the weak-anisotropy approximation and linearize the exact equations in the fracture weaknesses.

## Effective medium

The two fracture sets considered here (Figure 1) have microcorrugated surfaces and are described by the most general compliance matrix  $\mathbf{K}$  that has six independent elements (Grechka et al., 2003):

$$\mathbf{K} = \begin{pmatrix} K_N & K_{NV} & K_{NH} \\ K_{NV} & K_V & K_{VH} \\ K_{NH} & K_{VH} & K_H \end{pmatrix}, \quad (1)$$

where  $K_N$  is the normal compliance, and  $K_V$  and  $K_H$  are the tangential compliances. The off-diagonal compliance elements incorporate the influence of microcorrugation of fracture surfaces. For rotationally invariant fractures (penny-shaped cracks), the matrix (1) is diagonal and  $K_V = K_H$ .

Seismic signatures are convenient to describe in terms of normalized compliances called fracture *weaknesses*

## Signatures of microcorrugated fractures

(Grechka et al., 2003):

$$\Delta_N \equiv \frac{(\lambda + 2\mu) K_N}{1 + (\lambda + 2\mu) K_N}, \quad (2)$$

$$\Delta_J \equiv \frac{\mu K_J}{1 + \mu K_J}, \quad (3)$$

where the subscript  $J$  denotes either  $V$  or  $H$ . The off-diagonal weaknesses are defined as

$$\Delta_{IJ} \equiv \frac{\sqrt{\mu(\lambda + 2\mu)} K_{IJ}}{1 + \sqrt{\mu(\lambda + 2\mu)} K_{IJ}}, \quad (4)$$

where  $I$  and  $J$  stand for  $N$ ,  $V$ , and  $H$ .

According to the linear-slip formalism of Schoenberg (1980), the stiffness matrix  $\mathbf{c}$  of the effective model is obtained by adding the compliance matrices of the two corrugated fracture sets to that of the background and inverting the resulting matrix. The matrix  $\mathbf{c}$  linearized in the fracture weaknesses is given by

$$\mathbf{c} = \begin{pmatrix} c_{11} & c_{12} & c_{13} & \chi c_{24} & c_{15} & c_{16} \\ c_{12} & c_{22} & c_{23} & c_{24} & \chi c_{15} & c_{26} \\ c_{13} & c_{23} & c_{33} & \chi c_{24} & \chi c_{15} & c_{36} \\ \chi c_{24} & c_{24} & \chi c_{24} & c_{44} & 0 & c_{46} \\ c_{15} & \chi c_{15} & \chi c_{15} & 0 & c_{55} & c_{56} \\ c_{16} & c_{26} & c_{36} & c_{46} & c_{56} & c_{66} \end{pmatrix}; \quad (5)$$

$$\chi \equiv \frac{\lambda}{(\lambda + 2\mu)}.$$

According to equation (5), the effective model has the most general, triclinic symmetry (i.e., it does not have axes of rotational symmetry or symmetry planes), with only one vanishing elastic constant,  $c_{45} = c_{54}$ . Nonetheless, only 14 out of the 20 elastic constants are independent because the effective model is constructed using two Lamé parameters of the isotropic background ( $\lambda$  and  $\mu$ ) and 12 fracture compliances (six for each fracture set). If the fracture azimuth is unknown, it is also necessary to introduce an orientation angle that defines the azimuth of one of the sets.

### Shear-wave splitting

The shear-wave splitting coefficient ( $\gamma^S$ ) at vertical incidence is defined as

$$\gamma^S \equiv \frac{V_{S1}^2 - V_{S2}^2}{2V_{S2}^2}, \quad (6)$$

where  $V_{S1}$  is the velocity of the fast shear wave. Applying the second-order perturbation theory in terms of the

fracture weaknesses yields

$$\gamma^S \approx \frac{1}{2} \left\{ (\Delta_{V1} - \Delta_{V2})(1 + \Delta_{V1} - \Delta_{V2}) - g_b \left[ (\Delta_{VH1}^2 - \Delta_{VH2}^2) + (\Delta_{NV1}^2 - \Delta_{NV2}^2) \frac{(3 - 4g_b)}{1 + g_b} \right] \right\}, \quad (7)$$

where  $g_b \equiv V_{Sb}^2/V_{Pb}^2$  is the squared ratio of the background S- and P-wave velocities. As expected,  $\gamma^S$  at vertical incidence vanishes when the two fracture sets are identical. To the first order  $\gamma^S$  coincides with the splitting coefficient for rotationally invariant fractures, which is controlled by the difference between the fracture densities of the two sets (i.e., by the difference between the tangential weaknesses  $\Delta_{V1}$  and  $\Delta_{V2}$ ). However, if the second-order terms are substantial,  $\gamma^S$  is also influenced by the off-diagonal weaknesses  $\Delta_{VHi}$  and  $\Delta_{NVi}$  ( $i = 1, 2$ ). Note that the weakness  $\Delta_{NVi}$  depends on saturation and takes different values for fractures filled with gas, brine, or oil (Bakulin et al., 2000). Therefore, the vertical-incidence splitting coefficient for microcorrugated fractures with relatively large off-diagonal weaknesses may serve as an indicator of fluid saturation.

As illustrated by Figure 2, the exact coefficient  $\gamma^S$  can vary by as much as 50% over the entire range of plausible values of  $\Delta_{NV1}$  ( $\Delta_{NV2}$  was fixed). For a tight (non-porous) host rock,  $\Delta_{NV1} = 0$  corresponds to fractures filled with incompressible fluid such as brine, whereas nonzero values of  $\Delta_{NV1}$  describe fractures at least partially saturated with gas (Bakulin et al., 2000). If the host rock has pore space hydraulically connected to the fractures, the weaknesses  $\Delta_{NVi}$  do not necessarily vanish even for incompressible saturating fluids. Hence, for porous rocks the variation of  $\gamma^S$  with saturation may be less pronounced than that suggested by Figure 2. Also,  $\gamma^S$  becomes less sensitive to the off-diagonal compliances and saturation for softer rocks (e.g., marine sediments) with smaller values of  $g_b$ .

### NMO ellipses for horizontal reflectors

Important information for fracture detection is provided by reflection traveltimes, in particular by normal-moveout (NMO) ellipses, which can be represented as

$$V_{\text{nmo}}^{-2}(\alpha) = W_{11} \cos^2 \alpha + W_{12} \sin 2\alpha + W_{22} \sin^2 \alpha, \quad (8)$$

where  $V_{\text{nmo}}$  is the NMO velocity measured for the azimuth  $\alpha$ , and  $\mathbf{W}$  is a symmetric  $2 \times 2$  matrix. For a homogeneous layer of arbitrary symmetry,  $\mathbf{W}$  can be found from the Christoffel equation (Grechka et al., 1999). To analyze the NMO ellipses in a horizontal layer with two orthogonal, microcorrugated fracture sets, we linearized the exact equations in the fracture weaknesses [equations (2)–(4)].

## Signatures of microcorrugated fractures

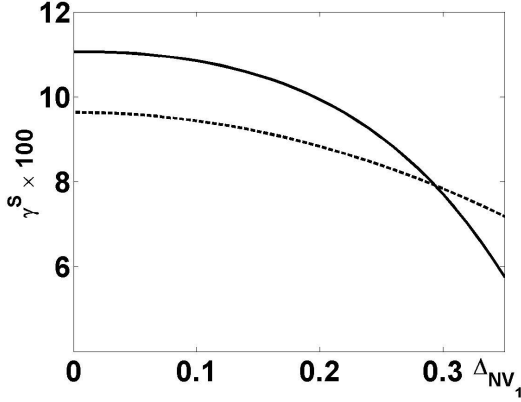


Fig. 2: Variation of the vertical shear-wave splitting coefficient  $\gamma^S$  as a function of the weakness  $\Delta_{NV_1}$ . The solid line is the exact  $\gamma^S$  from equation (6), where the velocities are computed from the Christoffel equation; the dashed curve is the approximation (7). The model parameters are  $V_{Pb} = 3$  km/s,  $V_{Sb} = 1.5$  km/s,  $\Delta_{N_1} = 0.5$ ,  $\Delta_{V_1} = \Delta_{H_1} = 0.25$  and  $\Delta_{NH_1} = \Delta_{VH_1} = 0.1$ . Each weakness of the second fracture set except for  $\Delta_{NV_2}$  is equal to one-third of the corresponding weakness of the first set;  $\Delta_{NV_2} = \Delta_{NH_1}/3$ .

For P-waves, the elements of matrix  $\mathbf{W}^P$  are:

$$W_{11}^P = V_{Pb}^{-2} \left[ 1 + \Delta_{N_1} (1 - 4g_b^2) + \Delta_{N_2} (1 - 2g_b)^2 + 4g_b \Delta_{V_1} \right], \quad (9)$$

$$W_{12}^P = 2V_{Pb}^{-2} (\Delta_{NH_1} + \Delta_{NH_2}) (1 - 2g_b) \sqrt{g_b}, \quad (10)$$

$$W_{22}^P = V_{Pb}^{-2} \left[ 1 + \Delta_{N_2} (1 - 4g_b^2) + \Delta_{N_1} (1 - 2g_b)^2 + 4g_b \Delta_{V_2} \right]. \quad (11)$$

Equations (9)–(11) show that only the presence of the off-diagonal weaknesses can explain the misalignment of the P-wave NMO ellipse with the fracture planes. If both fracture sets were rotationally invariant, the matrices  $\mathbf{W}$  for all three modes (not just for P-waves) would be diagonal, and the axes of the NMO ellipses would be parallel to the fracture strike directions. By contrast, for microcorrugated fractures all three NMO ellipses generally have different orientations, and none of them is aligned with the fracture azimuths (Figure 3). For the model in Figure 3, the weak-anisotropy approximations for the NMO ellipses (not shown here) are close to the exact solutions for the full range of azimuths.

The orientation of the NMO ellipse of the  $S_1$ -wave can help to distinguish between the models with one or two microcorrugated fracture sets. If the second set does not exist, then the semi-major axis of the NMO ellipse of the  $S_1$ -wave is parallel to both the fracture strike and the fast shear-wave polarization direction (Grechka et al., 2003).

### P-wave reflection coefficient

Another seismic signature that can be effectively used in

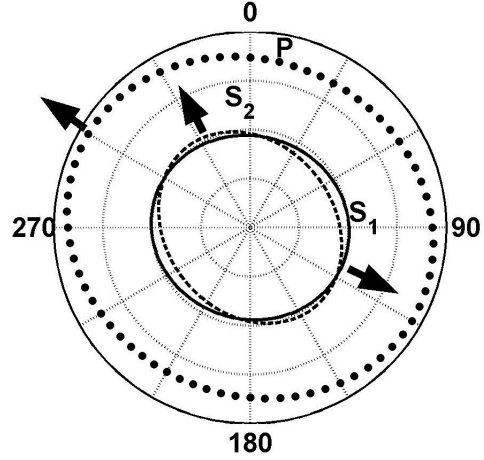


Fig. 3: Exact NMO ellipses for a horizontal layer that contains two vertical, orthogonal sets of microcorrugated fractures. The semi-major axes of the ellipses are marked by arrows. The strike azimuth of the dominant (first) fracture set is  $90^\circ$ . The parameters are  $V_{Pb} = 2$  km/s,  $V_{Sb} = 1$  km/s,  $\Delta_{N_1} = 0.25$ ,  $\Delta_{V_1} = \Delta_{H_1} = 0.12$ ,  $\Delta_{NV_1} = \Delta_{NH_1} = 0.17$ , and  $\Delta_{VH_1} = 0.12$ . Each weakness of the second fracture set is equal to one-third of the corresponding weakness of the first set.

fracture detection is the azimuthally varying reflection coefficient, in particular the AVO (amplitude variation with offset) gradient responsible for small- and moderate-offset reflection amplitudes. We consider an isotropic incidence halfspace above the triclinic medium described by equation (5) and assume a weak contrast in the elastic properties across the interface and weak anisotropy (i.e., small fracture weaknesses) in the reflecting halfspace. The weak-contrast, weak-anisotropy approximation for the P-wave reflection coefficient in arbitrary anisotropic media is derived in Vavryčuk and Pšenčík (1998). By combining their general result with the linearized stiffness coefficients for our model, we find the P-wave reflection coefficient  $R_{PP}$  as a function of the phase incidence angle  $\theta$ :

$$R_{PP}(\theta) = A + B \sin^2 \theta + C \sin^2 \theta \tan^2 \theta. \quad (12)$$

Here,  $A$  is the normal-incidence reflection coefficient that is not influenced by anisotropy,  $B$  is the AVO gradient, and  $C$  is the so-called “curvature” (large-angle) term. Both  $B$  and  $C$  can be separated into the isotropic and anisotropic parts, with the anisotropic part of the AVO gradient ( $B_{\text{ani}}$ ) obtained as

$$B_{\text{ani}}(\phi) = g_b \left\{ -[(1 - 2g_b) \Delta_{N_1} + \Delta_{V_1}] \cos^2 \phi - \frac{1}{2\sqrt{g_b}} (\Delta_{NH_1} + \Delta_{NH_2}) (1 - 2g_b) \sin 2\phi + [\Delta_{V_2} - 2\Delta_{V_1} - (1 - 2g_b) \Delta_{N_2}] \sin^2 \phi \right\}, \quad (13)$$

where  $\phi$  is the azimuthal phase angle measured from the  $x_1$ -axis. There are interesting similarities between equation (13) and equations (9)–(11) for the P-wave NMO

## Signatures of microcorrugated fractures

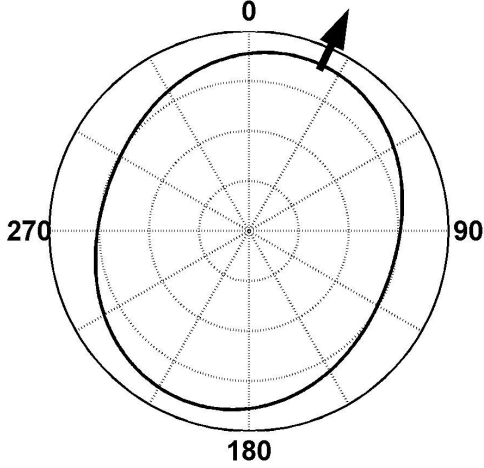


Fig. 4: Azimuthal variation of the P-wave AVO gradient for our triclinic model computed from equation (13). The strike azimuth of the dominant fracture set is  $90^\circ$ ; the direction of the largest gradient (black arrow) is close to  $25^\circ$ . The parameters are  $V_{Pb}/V_{Sb} = 3$ ,  $\Delta_{N_1} = 0.25$ ,  $\Delta_{V_1} = \Delta_{H_1} = 0.12$ , and  $\Delta_{NH_1} = 0.05$ . Each weakness of the second fracture set is equal to one-third of the corresponding weakness of the first set.

ellipse. First,  $B_{\text{ani}}(\phi)$  traces out a curve close to an ellipse in the horizontal plane, with  $B_{\text{ani}}^{-2}(\phi)$  being exactly elliptical. Second, the only off-diagonal weaknesses appearing in the linearized equations for both the reflection coefficient and NMO ellipse are  $\Delta_{NH_1}$  and  $\Delta_{NH_2}$ . Third, the “principal direction” of the curve  $B_{\text{ani}}(\phi)$  is rotated with respect to the horizontal coordinate axes (i.e., with respect to the fracture azimuths) only when  $\Delta_{NH_1} \neq 0$  or  $\Delta_{NH_2} \neq 0$ . Furthermore, the rotation angle of both the NMO ellipse and AVO gradient is controlled by the sum  $\Delta_{NH_1} + \Delta_{NH_2}$ .

The example in Figure 4 illustrates the orientation and the quasi-elliptical shape of the AVO gradient from equation (13). If the weaknesses  $\Delta_{NH_1}$  and  $\Delta_{NH_2}$  are set to zero, the direction of the largest (by absolute value) AVO gradient is perpendicular to the dominant fracture set. Despite the small values of  $\Delta_{NH_1}$  and  $\Delta_{NH_2}$ , the contribution of the off-diagonal weaknesses is sufficient for rotating this direction by about  $25^\circ$ .

### Discussion and conclusions

We studied seismic signatures of an effective triclinic medium formed by two sets of vertical, orthogonal fractures with microcorrugated surfaces embedded in isotropic host rock. By applying expansions in the fracture weaknesses (normalized compliances), we derived closed-form analytic expressions for shear-wave splitting, the NMO ellipses of horizontal reflection events, and the

P-wave reflection coefficient. Due to the presence of the off-diagonal weaknesses related to the roughness of fracture surfaces, the vertical shear-wave splitting coefficient  $\gamma^S$  varies with fluid saturation, and the NMO ellipses of all three modes are rotated with respect to the fracture strike directions and one another. For P-waves, the principal azimuthal directions of both the NMO ellipse and AVO gradient depend on the sum of the off-diagonal weaknesses  $\Delta_{NH_1}$  and  $\Delta_{NH_2}$ . If  $\Delta_{NH_1} = \Delta_{NH_2} = 0$ , then the NMO ellipse and AVO gradient are aligned with the fracture strike directions, as is always the case for penny-shaped cracks.

Although the fracture compliances for our model cannot be resolved individually even from the complete stiffness matrix (Grechka and Tsvankin, 2003), our results can help to estimate certain parameter combinations and verify whether the underlying physical model is appropriate. For example, analysis of the NMO ellipse of the fast shear wave  $S_1$  suggests a simple way to distinguish between models with one and two microcorrugated fracture sets. For a single set of fractures, the semi-major axis of the  $S_1$ -wave NMO ellipse and the polarization vector of the  $S_1$ -wave at vertical incidence are parallel to each other and to the fracture strike. This is no longer the case for the model with two fracture sets where the angle between the polarization vector and the semi-major axis of the NMO ellipse for the  $S_1$ -wave can reach  $20$ - $30^\circ$ .

### References

- Bakulin, A., Grechka, V., and Tsvankin, I., 2000, Estimation of fracture parameters from reflection seismic data - Parts I, II, and III: *Geophysics*, **65**, 1788–1830.
- Cardona, R., 2002, Fluid substitution theories and multi-component seismic characterization of fractured reservoirs: Ph.D. thesis, Colorado School of Mines.
- Grechka, V., Bakulin, A., and Tsvankin, I., 2003, Seismic characterization of vertical fractures described as general linear-slip interfaces: *Geophysical Prospecting*, **51**, 117–129.
- Grechka, V., and Tsvankin, I., 2003, Feasibility of seismic characterization of multiple sets: *Geophysics*, **68**, 1399–1407.
- Grechka, V., Tsvankin, I., and Cohen, J. K., 1999, Generalized Dix equation and analytic treatment of normal-moveout velocity for anisotropic media: *Geophysical Prospecting*, **47**, 117–148.
- Schoenberg, M., 1980, Elastic wave behavior across linear slip interfaces: *Journal of Acoustical Society of America*, **68**, 1516–1521.
- Vavryčuk, V., and Pšenčík, I., 1998, PP-wave reflection coefficients in weakly anisotropic elastic media: *Geophysics*, **63**, 2129–2141.